Inrush Current Measurement for Transient Space Characterization and Fault Detection

Erik K. Saathoff, *Graduate Student Member, IEEE*, Daisy H. Green, *Graduate Student Member, IEEE*, Rebecca A. Agustin, Joseph W. O'Connell, and Steven B. Leeb, *Fellow, IEEE*

***Abstract*— Training the load identification algorithm for a power-system monitor (PSM) begins with characterization or observation of the loads. This article demonstrates a phase-controlled switch that, *in situ*, accounts for the effects of source and line impedance on load transients at controllable phase angles with respect to the ac voltage line-cycle. The phase angle significantly affects the inrush for many loads, such as lighting, induction motors, and power supplies. The circuitry and signal identification techniques presented in this article can provide a full set of training data for machine learning algorithms for power system monitoring. The system can also be used as the foundation of a "smart switch" in grid applications for automatic demand response control.**

***Index Terms*— Condition monitoring, fault detection, monitoring.**

I. Introduction

MANY electrical loads, such as lighting, induction motors, and power supplies, can draw large inrush currents, which in some cases may exceed ten times the steady-state power. The nature and characteristics of the inrush are dependent on the physical construction of the load. Load transients are important characteristics that can serve as a "fingerprint" for identifying loads and load pathologies with machine learning techniques [1], [2]. Inrush current varies with load condition, load state, and the utility line cycle. The phase angle of the electric utility shapes inrush current, and can produce profound differences in size, duration, and shape for some loads. Characterizing a load's inrush transient can allow for load identification, and can further be used for diagnostic evaluation of equipment using power-system monitors (PSMs) [3]–[6]. Prompt identification of impending faults is especially important for mission-critical systems where system reliability is critical [7].

It is difficult to trust a machine pattern classifier output if training data does not include a full characterization of the monitored loads. To reliably train a PSM for load diagnostics and condition-based maintenance (CBM), informed decision or pattern classification boundaries are necessary, especially as a load's behavior changes over time due to aging or degradation. These changes or deviations in power may indicate the beginning of a "soft fault," or the gradual degradation of equipment performance. Both normal and degraded load signatures vary with line interactions. Also, in the field, grid performance differs from a lab's, affecting the size, shape, harmonics, and time constants of a load's inrush transient. Various load signature databases exist which offer a convenient avenue for load identification training [8]–[11]. However, these databases may not adequately map the behavior of a load, and often only include healthy behavior. Inaccurate or incomplete characterization of load transients compromises the fidelity of load identification.

Test equipment [12], [13], especially synthesized ac power supplies, can be used for inrush and load testing. These ac sources typically work well for loads with relatively light transient demands. They may not produce realistic load signatures for more demanding loads. In addition, the line impedance between a load and its source affects the transient. To achieve best results for a machine pattern classifier, a full phase-controlled switch is necessary to perform *in situ* testing. By deploying the switch conveniently into an existing utility connection, the effects of the real source and line are included in the data. The resulting exemplar data will be a closer match to what a PSM will observe, and can improve the fidelity of load identification. This switch can turn on the load at a desired phase angle of the utility voltage, permitting simplified sweeps over the turn-on angle. The switch should exhibit minimal insertion impedance to avoid altering load transients. Meziane *et al.* [14] and Renaux *et al.* [15], [16] present related hardware that can control the turn-on phase angle of the load. These systems are simply used as an alternative to synthesized ac power sources, and the works do not consider the effect of source and line impedance on inrush measurements. This article demonstrates the use of a phase-controlled switch, tailored for smart control and monitoring applications, for generating the transient feature space of various lab loads under both healthy variations and fault scenarios.

II. Smart Switch

Fig. 1 presents a simplified schematic of the TRIAC-based phase-controlled switch used to generate inrush transients in

Manuscript received March 1, 2021; revised April 27, 2021; accepted May 25, 2021. Date of publication June 14, 2021; date of current version July 6, 2021. This work was supported in part by The Grainger Foundation, in part by the Office of Naval Research NEPTUNE Program, and in part by MathWorks. The Associate Editor coordinating the review process was Tarikul Islam. *(Corresponding author: Erik K. Saathoff.)*

The authors are with the Department of Electrical Engineering and Computer Science, Massachusetts Institute of Technology, Cambridge, MA 02139 USA (e-mail: saathoff@mit.edu; dhgreen@mit.edu; agustinr@mit.edu; joeyoc@mit.edu; sbleeb@mit.edu).

Digital Object Identifier 10.1109/TIM.2021.3089226

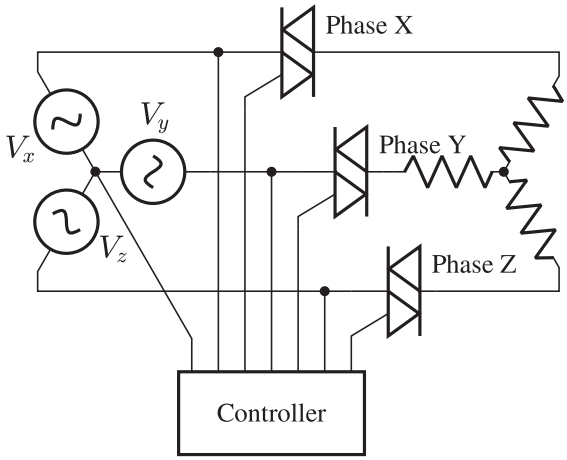

Fig. 1. Three-phase diagram of the source, switch, and load [18].

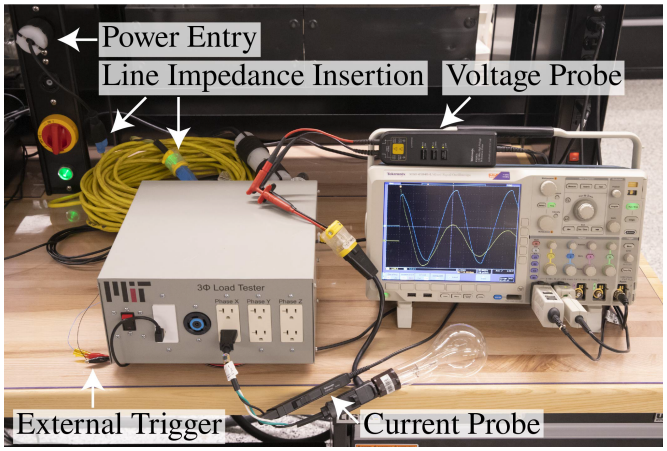

Fig. 2. High-speed inrush measurement setup.

this article. A TRIAC's controllable turn-on makes this switch a useful choice for inrush testing. The switch can power both three-phase loads and an arrangement of single-phase loads. The semiconductor power devices introduce some non-idealities due to voltage drop, incremental resistance, parasitic series inductance, and gate drive dynamics. These effects produce very little distortion in the inrush current and will not affect the demonstration of inrush transient variability. The testing performed here can be extended to other semiconductor switch arrangements including MOSFETs and GaN FETs. Other types of switches may reduce parasitic effects compared to the TRIAC and provide additional test behavior. For instance, the bouncing contacts [17] of physical switches can be emulated with semiconductors that can turn the load on and off rapidly.

Each TRIAC is controlled by a Cypress Semiconductor PSoC 5LP microcontroller (MCU) through galvanically isolated signal interfaces. A polarity detector reports whether the phase voltage is above the neutral, and the MCU uses this to time the turn-on event for any of the phases. Specifically, the turn-on phase angle is defined starting at the positive-slope zero-crossing of the line voltage. A positive-edge-triggered delay counter in the MCU connected to the polarity detector performs the timing in increments of 250 ns. Each phase can handle up to 30 A of continuous current and 120 V from phase-to-netural. While the phase-controlled switch used in this article is a piece of test equipment, it is also deployable as a "smart" switch for distributed real-world testing.

III. Experimental Setup

Inrush testing performed in Section IV and Section VI-A was completed with the setup in Fig. 2. This setup pulls one phase from a three-phase power receptacle, and allows a single-phase utility cable to be inserted into the utility connection to add line impedance. Three pieces of Tektronix equipment measure the load voltage and current: a TCP0030A current probe, P5205A differential voltage probe, and MSO4104B-L oscilloscope. The oscilloscope samples at 25 Msps in high resolution mode. The high sampling rate allows for inspection of the waveforms down to the microsecond level. The MCU outputs a trigger signal to the oscilloscope to keep the turn-on point consistent. The waveform data is transferred to a computer and used to generate the plots without post-processing.

To explore transient space variability in Section V and to explore fault detection and diagnostics in the remainder of Section VI, a PSM, specifically a Nonintrusive Load Monitor (NILM), was used to measure power of the loads controlled by the phase-controlled switch. Using nonintrusive load monitoring allows for measurements at a central location in a power grid. The three-phase voltages and currents are sampled at 8 ksps, then processed into 60 Hz real power (P) and reactive power (Q) with the Sinefit algorithm [19]. This high sampling allows the measurement of transient shapes. This setup utilizes the LEM LF-305S current transducers and LEM LV-25P voltage transducers.

IV. Inrush Testing: Sources of Distortion

Especially for loads with large inrush transients, the impedance of the electrical source can substantially affect the inrush. Performing an inrush test without regard to the system source and line implementation can result in waveforms with different characteristics from those found in practice. These differences may cause PSM load identification algorithms to mis-identify loads. This section demonstrates these effects and illustrates how the phase-controlled switch can provide satisfactory test data for reflecting realistic load and grid performance.

A. Source Effects

Synthesized ac power supplies can act as controlled sources for inrush current testing. These sources do not realistically model line impedance, and they have limitations on the peak current they can deliver. Inrush data collected with test equipment may, therefore, fail to model observations in the field.

Fig. 3 shows the turn-on transient of a 155-Ω wire-wound resistor connected to a commercial ac source. This test

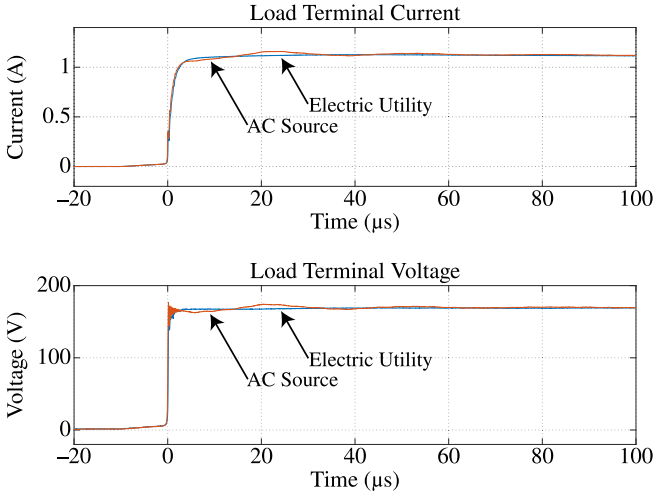

Fig. 3. Voltage and current waveforms for a 155-Ω resistor turn-on using either an ac power supply or the electric utility as the source [20].

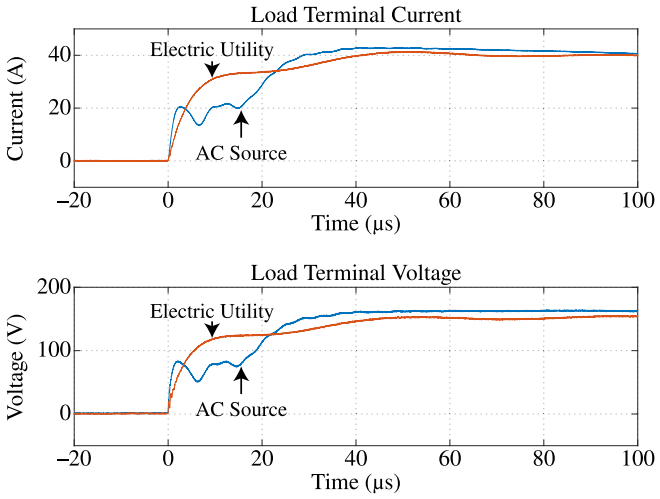

Fig. 4. Voltage and current waveforms for a 250-W incandescent lamp turn-on using either an ac power supply or the electric utility as the source [20].

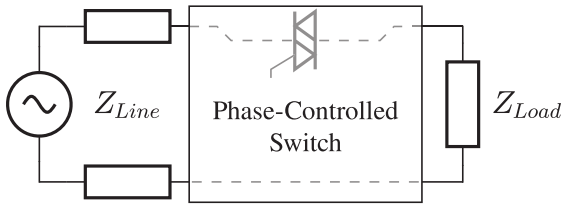

Fig. 5. Model of the source connection as a Thevenin voltage source with series impedance elements.

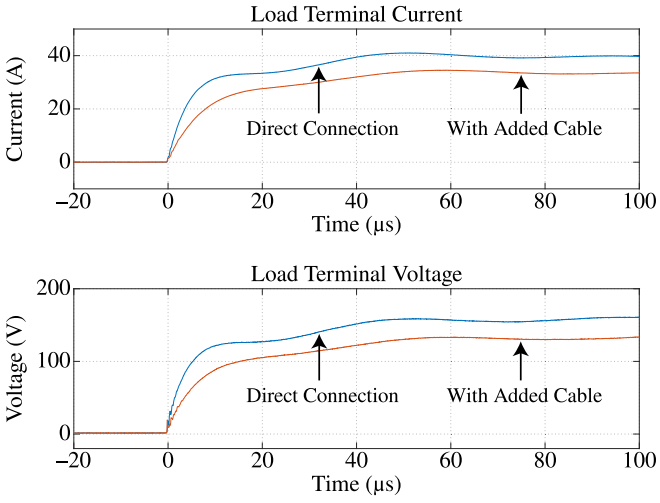

Fig. 6. Voltage and current waveforms for a 250-W incandescent lamp turn-on with or without added line impedance using the electric utility as a source [20].

makes use of the source's ability to enable the output at a desired angle of 90°. Here, an Agilent 6834B configured for single-phase output, 120 V_{rms}, and 30 A_{rms} current limit is used. Other tests in this article that use the commercial ac power supply will use this same configuration. A transient is also generated using the phase-controlled switch and with the electric utility as the power source at the same turn-on angle. In this case, the ac source and phase-controlled switch generate similar transients. The high current-rise time causes some oscillations in the power supply's feedback loop, but the shape of the current remains similar in both cases. After only 50 μs, both sources provide an almost perfect match.

However, many loads present current demands that challenge the capabilities of an ac power supply. Many loads begin their inrush by presenting a low impedance to the utility, maximizing current magnitude and slew rate. These loads include rectifiers energizing bus capacitors and incandescent lamps. A 250-W incandescent lamp has a steady state power consumption that is a small fraction of the commercial ac source's capacity. However, the worst case peak current consumed during the transient is nearly 100% of the peak current limit. This worst case occurs at the peak of the line voltage, i.e., a turn-on angle of 90°.

Fig. 4 shows the resulting transient when switching on a 250-W incandescent lamp at a 90° turn-on angle. The voltage generated by the commercial ac power supply is well below the expected 170 V during the initial 25 μs of the transient. In contrast, the phase-controlled switch does not introduce its own distortions into the observed load behavior. The resulting currents, which would be inspected by a PSM, also differ greatly at the beginning of the inrush. As the load demand stabilizes and the ac source's energy-storage elements recover, the two waveforms begin to match up. Active loads containing grid-connected power electronics can generate a series of fast current steps, each of which could generate a similar voltage distortion when powered by the commercial ac source. The phase-controlled switch, when powered with a stiff, stable source, can produce more realistic results.

B. Line Impedance Effects

Performing inrush testing with a lab's electric utility will prevent distortion caused by an ac source, but the line impedance also affects the results and will be different in the field. Line impedance, as shown in Fig. 5, prevents

loads from drawing arbitrarily large and fast current pulses. In particular, line inductance will have the largest impact during high (di/dt) steps and will significantly smooth out high-speed transients. Additional resistance will mainly affect high current transients, and will reduce the overall magnitude. To demonstrate this effect, a 30.5-m (100-ft) single-phase utility cable is placed between the phase-controlled switch and the electric utility connection. With this extra line impedance in the system, the phase-controlled switch turns the same incandescent lamp on at a 90° turn-on angle. Performing this test at the voltage peak will create the fastest possible current rise and thus the largest interaction with the new line inductance.

Fig. 6 shows the inrush transient both with and without the single-phase utility cable placed between the switch and the electric utility. The additional line impedance significantly affects the voltage and current delivered to the load. The additional inductance reduces in initial current slew rate, and the additional resistance decreases the overall magnitude. The changes also affect the resonant frequency of the line, decreasing the frequency of the voltage oscillations.

A line impedance network may be used to perform the inrush current testing, but determining the arrangement and values of components to create an accurate representation is difficult. Using a simplified *R-L* line model is typically sufficient, but it may not capture all relevant dynamics. For example, the voltage oscillations in Fig. 6 indicate the presence of line capacitance. Recreating these dynamics requires choosing a complicated model and matching it to measured data. An alternative is to perform the testing *in situ* in the electrical environment of interest. A phase-controlled switch can be spliced into a target load's utility connection, and the data generated will be more realistic and will not provide opportunities for modeling error.

V. Transient Variability Space

PSMs recognize the consumption signatures of electrical loads. Classes of loads have certain electrical characteristics that can serve as fingerprints for load identification. By training a PSM's load identification algorithms to identify these signatures, a PSM can interpret aggregate power flow as the operation of specific loads. The training to detect load turn-on events requires various inrush transient exemplars for each load. However, even for a healthy load, inrush transients vary due to factors such as turn-on phase angle, voltage amplitude, line conditions, operating conditions, and environmental factors. Testing should involve varying these parameters, and the resulting data forms a transient variability feature space for the load. A PSM must be able to identify all transients within a load's variability space for reliable load identification. Furthermore, these load transients can change over time due to aging and degradation, or underlying fault conditions. This expands the transient variability feature space and further complicates accurate load identification. By characterizing the transient feature space for both healthy and faulty behavior, a PSM can provide prognostic indicators of machine health.

For example, a PSM monitoring a 7.5-kW shipboard controllable pitch propeller (CPP) pump detected a slow change in the pump's steady-state power consumption over the course of four years correlating to the normalized operating pressure, as shown in Fig. 7(a). The PSM also detected a variation in the maximum inrush power of the CPP pump as shown in Fig. 7(b). However, this variation does not depend on time or trend with the changes in steady-state power. As a result, the PSM was able to characterize the load based on its inrush power and still identify the load. Understanding the feature space variations and their underlying causes is essential for equipment identification and diagnostics.

The choice of tool to generate a load's transient space is imperative for efficiency and completeness. It is important to perform the inrush tests in the same source and line environment as is used for normal operation. Splicing a switch in series with the load is the optimal technique. Mechanical switches, such as relays, have probabilistic actuation times of up to tens of milliseconds. Closing the switch also causes stochastic bouncing effects. Although such a switch is effective for controlling the cycling behavior of a load, the lack of accurate control over turn-on angle is problematic and the bouncing contacts create severe parasitics. Solid-state relays (SSRs) alleviate both the timing inconsistency and bouncing contacts, but are not useful without a controller monitoring the utility's electrical phase. In addition, many SSRs only actuate at zero-crossings, severely limiting the possible turn-on angles and thus the observable transient space.

The proposed phase-controlled switch acts as an excellent tool for transient space generation due to its accurate turn-on angle control, cycling control, and minimal parasitics. Other factors that affect the inrush transients are typically small or cannot be reasonably controlled. Testing multiple times at each operating point is generally the best method to examine load specific parameters, such as the starting orientation of a motor shaft. This section explores the transient variability using the phase-controlled switch on various lab loads.

A. Centrifugal Fan Feature Exploration

First, a 1-hp induction motor centrifugal fan serves to demonstrate how turn-on angle can affect inrush transient. The motor has a series capacitor on one of the two windings both during startup and while running. The phase-controlled switch starts the load at a selection of phase angles: 0°, 60°, 90°, 120°, and 180°. The input current produced when turning the fan on is shown in Fig. 8. Like most inductive loads, the centrifugal fan's worst case current is near the voltage zero-crossings. During startup, the core inductance of the machine significantly impacts the inrush current. The turn-on angle that can maximize the volt-second integral on the induction-machine model will generate the largest current, which happens when starting near a zero-crossing. However, the series capacitor will shift the position of the worst case somewhat.

It is also useful to view the power consumed by the load averaged over a line cycle rather than the pulsing current itself. The voltages and current can be converted to the phase fundamental power spectral envelope using the Sinefit algorithm for each phase current over each measured voltage

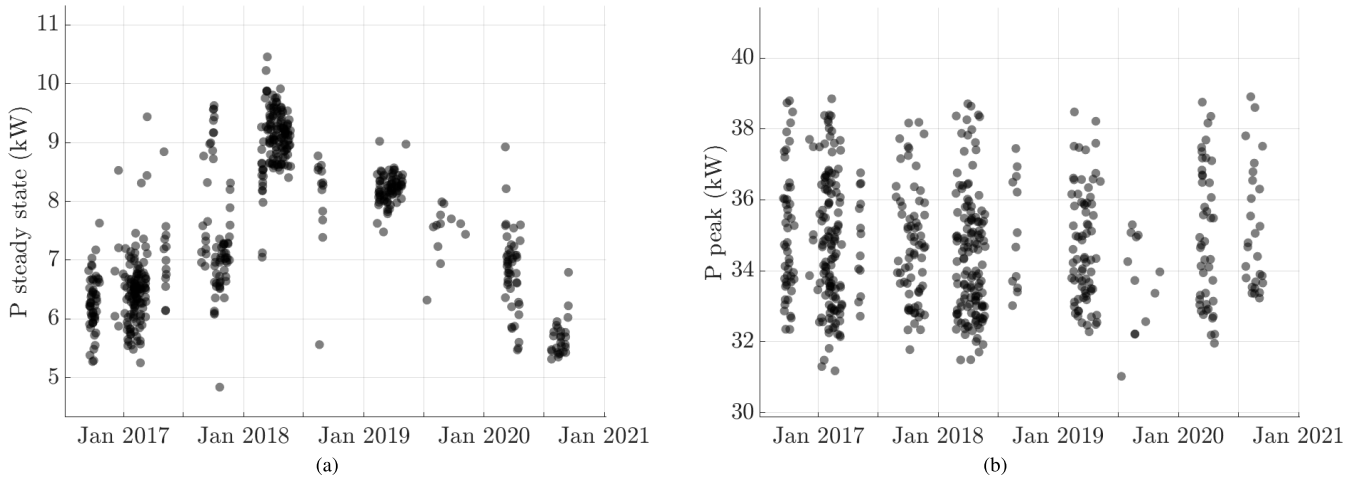

Fig. 7. CPP pump power draw trends over time. (a) Steady-state real power versus time. (b) Maximum real power inrush versus time.

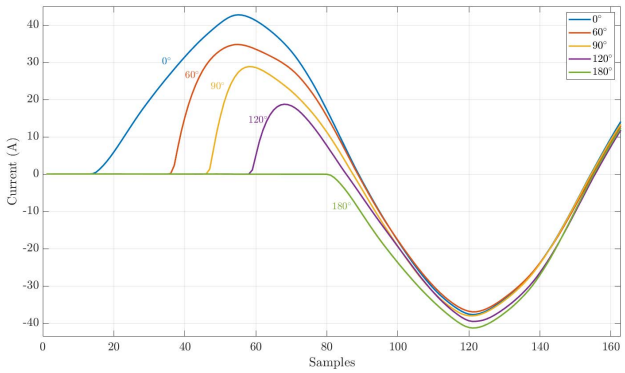

Fig. 8. Inrush current transient of the centrifugal fan at various turn-on angles.

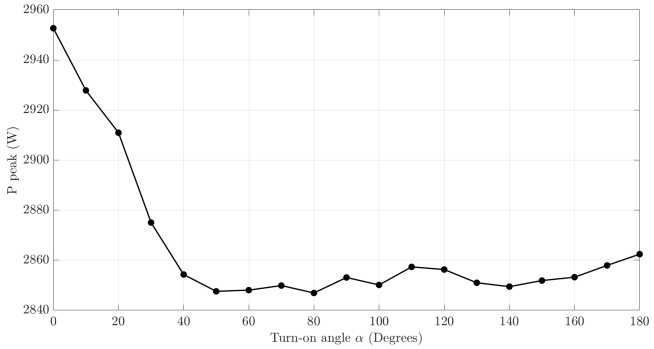

Fig. 9. Inrush power peak of the centrifugal fan for various turn-on angles.

line cycle [19]. Using this technique, the fan is activated ten times for each turn-on angle from 0° to 180° in increments of 10°. Fig. 9 shows the inrush real power of the fan as the average of ten activations for each turn-on angle. As expected, the maximum power inrush is at 0°.

B. Variable Speed Fan Feature Exploration

Other types of fans present significantly different inrush behavior. An electronic variable speed fan, due to its built in speed controller and large dc storage capacitance, acts as a good demonstration of how turn-on angle and cycling affect the inrush current transient. The fan has an electronically commutated motor (ECM) and uses a full-bridge rectifier to convert the ac input to dc. For testing consistency, the fan runs at its maximum speed. Similar to the centrifugal fan, the phase-controlled switch starts the load at a selection of phase angles: 0°, 60°, 90°, 120°, and 180°. The input current generated when turning the fan on is shown in Fig. 10. As is typical for rectifier and capacitor inputs, the fan draws significant current at turn-on. In contrast to the centrifugal fan-in which the current peaks at the voltage zero-crossings, the variable speed fan current inrush is highest when the voltage nears the peak; e.g., when the turn-on angle is close to 90° or 270°. When the turn-on angle is 0° or 180°, the initial voltage is zero and the current rises steadily from zero without any spiking. After the initial inrush, the fan continues to consume power in pulses during each half line cycle. The 0° and 180° cases also look very similar, with the latter being delayed by half a line period and inverted. Any load that does not have line voltage polarity dependence, such as this variable speed fan, will behave similarly. The inrush current for a turn-on angle of α will be the same as $\alpha + n180°$.

The fan is activated ten times for each turn-on angle from 0° to 180° in increments of 10°. This data aids the training of a PSM and the range of possibilities can be mapped quickly. The testing efficiently is greater than or equal to uncontrolled-phase-angle testing, as would be performed with an immediate-actuation SSR. After plotting the peak inrush power as a function of turn-on angle, regions of these plots with greater first and second derivatives can be identified. These regions should be captured in greater detail, and the phase-controlled switch makes this simple by permitting variable spacing between turn-on angles. Although the centrifugal fan peak inrush power generally decreases as the turn-on angle increases, the variable speed fan is non-monotonic. For the variable speed fan, the region between 60° to 90° contains large first derivatives. This region is retested a a smaller increment of 3°. Fig. 11 shows the resulting inrush power peak verses turn-on angle, with the original

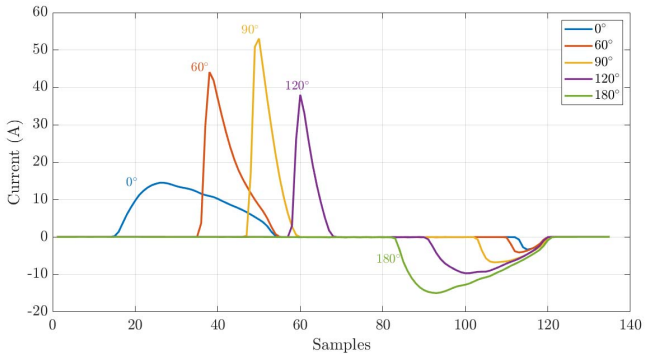

Fig. 10. Inrush current transient of the variable speed fan at various turn-on angles.

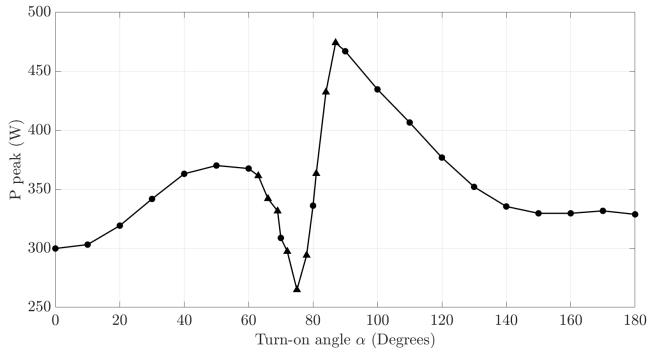

Fig. 11. Inrush power peak of the variable speed fan for various turn-on angles.

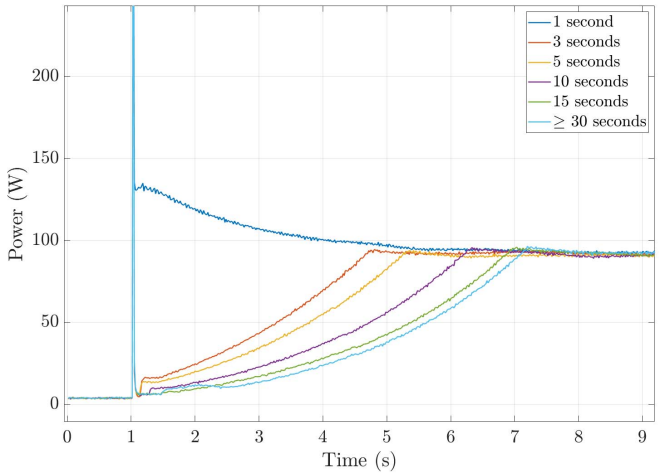

Fig. 12. Power envelope of the variable speed fan with varying off-time between load activations.

10° increments plotted with circles, and the greater resolution 3° increments plotted with triangles. This adaptive testing approach significantly improves on previous applications [14]–[16] of a phase-controlled switch for inrush testing which use fixed, coarse turn-on angle control.

The initial inrush changes based on the turn-on phase angle, as shown in Figs. 10 and 11. Thus, using the phase-controlled switch to keep the phase angle constant, the effects of other

Fig. 13. Incandescent lamp load with series resistance, along with an equivalent electrical model.

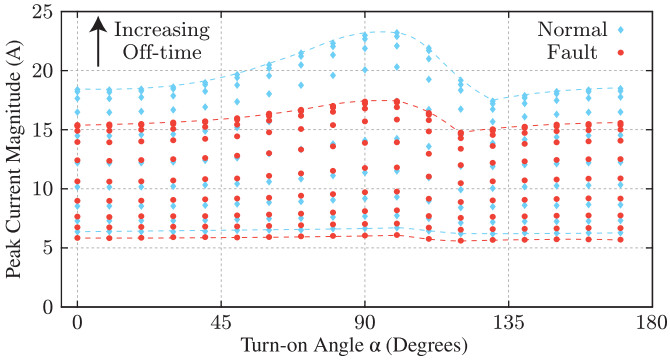

Fig. 14. Feature space for a 250-W incandescent lamp in series with a 3-Ω (normal) or 5-Ω (fault) resistor.

operating or environmental conditions can be tested. By changing how a load is cycled on and off, the turn-on waveform changes and provides more information about the load. The mechanical inertia, combined with the speed controller, causes different power draw signatures as the fan approaches steady state. Since this effect occurs over many line cycles, the power spectral envelope will be used again. Fig. 12 shows the full turn-on transient after variable times between an off-event and the next load activation. These tests are performed as an average of 15 transients at a turn-on angle of 75°. In each test, the transient starts with a large peak as the dc buffer capacitor is charged. Afterward, the speed controller draws a variable level of power depending on the starting conditions of the fan, e.g. the initial rotation speed of the fan. As the time between load activations increases, the time to reach stead state increases. This effect stops when the off-time exceeds 30 s, as this is the time required for rotational velocity to reach zero. Unlike the other cases, the 1 s off-time case does not drop to low power after the initial inrush spike, and instead consumes more than steady state power. The speed controller likely has both soft-start and running modes. In the 1 s case, the fan does not slow down enough to reach soft-starting territory, so the speed controller tries to quickly return to the correct speed.

VI. Transient Fault Detection and Diagnostics

The phase-controlled switch can also generate a load's inrush transient feature space for degrading behavior or other fault conditions. This enables a PSM to be able to identify a load in its unhealthy state. This section explores the transient variability of faulty loads using the phase-controlled switch on various lab loads.

A. Wiring Degradation Fault

Loads often appear to be working properly, even while severely degraded. To investigate how the phase-controlled

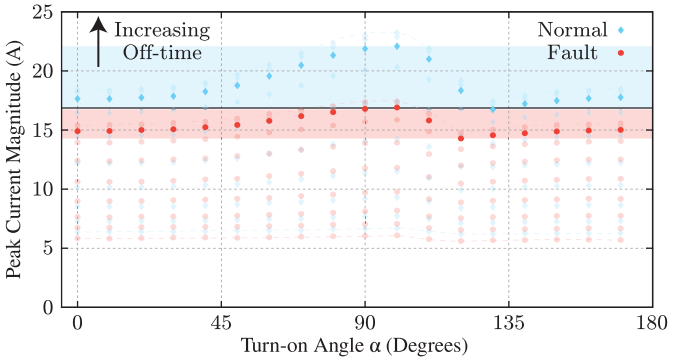

Fig. 15. Feature space for a 250-W incandescent lamp in series with a 3-Ω (normal) or 5-Ω (fault) resistor highlighting the 36-s off-time case.

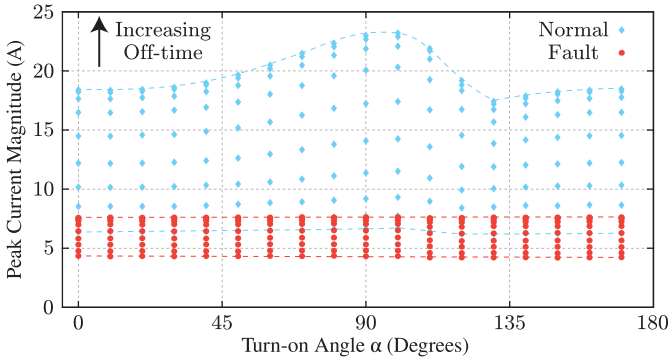

Fig. 16. Feature space for a 250-W incandescent lamp in series with a 3-Ω (normal) or 17-Ω (fault) resistor.

switch can generate useful data for fault detection, the idea of degrading wiring is applied to an incandescent lamp. The lamp's significant inrush transient will add interesting dynamics to this example. Fig. 13 shows the electrical model of the incandescent bulb load. R represents line resistance and any other series resistance associated with the load. To simulate a fault, a resistor of value R is placed in series with the load and varied. This added resistor is large compared to the measured line resistance. The lamp filament is represented as a variable resistance, r, which is extremely nonlinear. This value varies between about 4 Ω at room temperature, and 57 Ω when hot under normal line conditions.

Fig. 14 provides a visualization of a theoretical "soft" failure. The phase-controlled switch generates the space of possible transients for a fixed 3-Ω or 5-Ω resistor in series with a 250-W incandescent lamp. Transients are generated at half of the range of turn-on angles in 10° increments, and with the lamp turned off for one to one hundred seconds in logarithmic increments. The lamp is turned on for one second in each test which adequately allows the filament to reach equilibrium. For each turn-on angle, the range of peak-current magnitudes are plotted. Higher current peaks correspond to a longer off-time for the load. This makes physical sense, as the filament is cooler at the beginning of the test and thus r is smaller. An increase in resistance indicates some sort of electrical degradation. The 3-Ω case is considered normal, whereas the 5-Ω case corresponds to a fault.

The visualization demonstrates that the increased resistance in the fault case decreases the worst case peak current for all phase angles. This information alone can provide reliable feedback that the heater system is in good condition if a large enough current peak is detected. However, an extensive region of the feature space overlaps and more complicated identification techniques may be necessary to detect the fault. Since a PSM will know how long the load was off, it can isolate part of this space as shown in Fig. 15. Here, the load is turned off for approximately 36 seconds before the next actuation. The overlap is significantly reduced, and thus almost every inrush transient observed can be reliably binned into either being normal or faulty.

When the fault becomes more significant, the transient space in the fault case separates further from the normal case. Fig. 16 demonstrates this with a fault resistance of 17 Ω. The overlap is minimal and can be ignored if a healthy load will never be cycled off for only a few seconds. The dynamics of the incandescent lamp are significantly slower, removing variation with respect to α. In this fault scenario, an inrush transient can almost always be binned into either being normal or faulty without keeping track of load activation times. Since this type of fault significantly affects the inrush transient, load identification algorithms focused on the inrush will need fault-case training data to correctly identify the load as it strays further away from expected load behavior. This testing provides the exemplar data for such training.

B. Ventilation System Blockage

Loads experience changes in their overall power consumption due to degradation of system components. For example, PSMs can detect when a ventilation system has a leaky duct or clogged filter by observing changes in the fan's power consumption [21]. The variable speed fan is used in a ventilation set-up to explore the relationship between filter blockage and power consumption. To emulate blockages in an air ventilation system, 12.7-mm (0.5-in) Polyester Plastic MERV5 filters, with 3 micrometer permeability, are introduced on the intake side of the system. The variable speed fan from Section V-B is used to perform this test. Filters are successively introduced to simulate increased filter blockage, and finally total blockage is tested using cardboard, effectively reducing air flow to zero. At each blockage level, the fan is run once at each turn-on angle from 0° to 360° in increments of 10°.

Fig. 17 shows the inrush peak real power versus the steady-state power level for each run at various blockage levels. This fan is a constant rpm ECM, which means that the blades will spin at the same speed regardless of external static pressure changes. Based on the fan pressure curve [22], a small decrease in flow rate caused by the first two filters will cause a sharp increase in static pressure, increasing the torque on the motor shaft and raising the overall power consumption. However, the curve quickly flattens, resulting in lower torque for further flow restrictions. As more filters are added and the flow rates drops toward zero, the fan is no longer producing effective work. The shaft is only loaded by drag, causing the power consumption to decrease. The

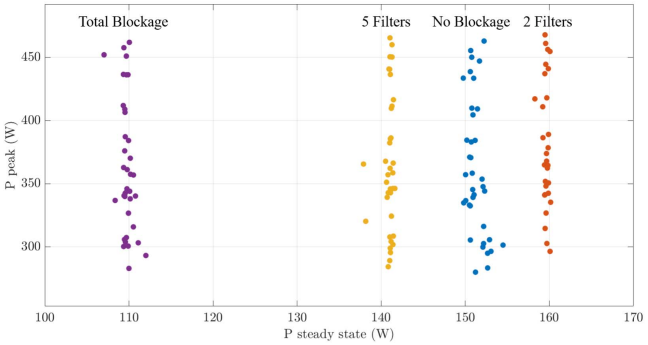

Fig. 17. Inrush power peak versus steady state for the variable speed fan with varying filter blockage levels.

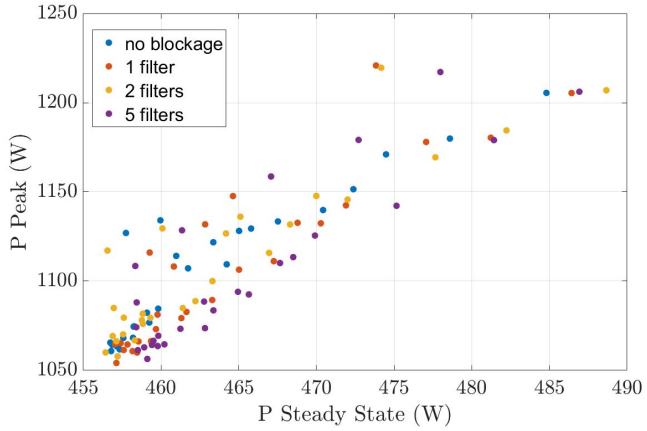

Fig. 18. Peak inrush and steady state power consumed by an axial fan at various blockage levels. Temperature decreases as points move up and to the right.

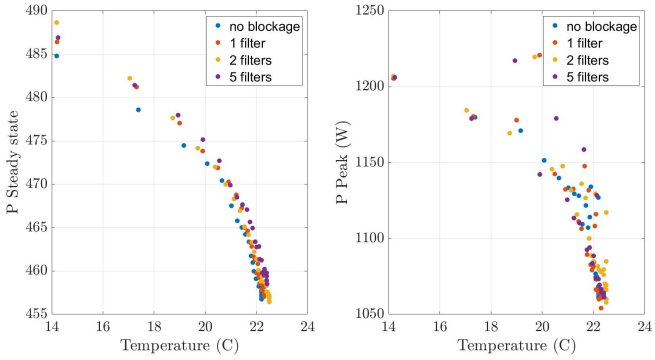

Fig. 19. Axial fan steady state real power (left) and peak inrush real power (right) versus temperature.

inflection point of the power curve, and the power difference between zero and full blockage, are dependent on the fan design. Constant flow rate ECM fans produce similar results, but their variable rpm operation can make the curve more exaggerated [23]. Despite the steady-state power changing as the blockage level increases, the range of peak power values does not change. This range of values is consistent with the peak power characterization in Fig. 11. The inrush transient of this load is dominated by the charging of the large internal dc capacitance, and this process is completed before a blockage can affect the fan blades. This series of tests, performed with the phase-controlled switch, confirms that a blockage fault does not affect the variability-space peak-power axis for this type of fan. Thus, a load identification algorithm focused on the inrush transient can recognize this load even as it experiences this type of fault without any additional training. It can further be used to diagnose the fault condition by observing the changing steady-state power levels.

C. Ventilation System Temperature Dependence

Investigation of a load's feature space can also extend into the environmental variables, such as temperature. A 0.7-hp single-phase axial fan driven by an induction motor is used in the same ventilation set-up as the variable speed fan. A permanent split capacitor motor, such as this axial fan, does not have a speed controller to maintain a constant rpm. Thus, normally when the external static pressure of the system changes it leads to power changes based on the fan's characteristic fan curve. [24]. However, this fan does not exhibit significant changes in steady-state power based on filter blockage. Instead, the fan's power draw exhibits a significant temperature dependence. A majority of loads do not operate under strict temperature control and their temperature may change with both the ambient and internal heating. Motors generate heat from various losses, which will slowly increase their temperature until they reach steady state with the ambient. A high thermal mass leads to long thermal time constants, and thus investigating inrush at different temperatures is useful. Since the rotor bars in an induction machine change conductivity with temperature, the power consumed should also change during a turn-on transient.

An experiment is performed in which the axial fan ventilation setup is subjected to colder temperatures, then starts with a random turn-on angle for 27 runs each at various filter blockage levels. Fig. 18 shows the inrush peak power versus the steady-state power level for each run. There is no clear dependence of the steady-state power level on filter blockage, as is the case for the variable speed fan, as shown in Fig. 17. Instead, both the steady-state and peak power depend on the temperature, as shown in Fig. 19. Here, the temperature is measured at the outlet of the ventilation system. As the system warms up, the steady state and inrush power both decrease. This additional information can improve load identification algorithms by including new extremes on expected operating behavior. In addition, the lack of dependence on blockage contrasts with the previous ventilation example, indicating that correlations between load variables are not necessarily universal and must be characterized for each load. Incorrectly applying assumptions to this duct fan can result in mistakenly attributing a decrease in power to a leaky duct, rather than a hot motor. The temperature dependence can also be used as a diagnostic indicator of the associated temperature control system or the fan itself, as increased temperature can indicate a winding short, failed bearing, or other lossy faults.

VII. Conclusion

High-quality inrush current testing is essential for many design, monitoring, and fault detection applications. Conventional testing with commercial ac power supplies may not adequately capture the variables that affect real-world inrush transients. This article discusses the use of a phase-controlled switch which can be deployed on real-world source connections. The inclusion of source and line impedance from the target environment improves the quality of the results.

The phase-controlled switch has been demonstrated as an effective tool for characterizing a load's inrush behavior. The control over turn-on angle allows a user to sweep a range deterministically rather than randomly. Ranges of angle with interesting behavior can be isolated or swept with finer granularity. Load cycling can also be independently controlled to investigate the relationship with turn-on angle. By removing random variables, additional testing can be performed more thoughtfully and completely. Overall, this testing forms a inrush-transient feature space for the load. This testing is extended to include fault scenarios, as these can widen the variability space and require changes to the load identification algorithm. Further, diagnostics can be performed by tracking changes in the load's behavior over time. When the phase-controlled switch is deployed as a "smart" switch, new exemplar data can be generated as the load is actuated, providing useful field data and tracking deviations in load behavior.

References

[1] F. Ciancetta, G. Bucci, E. Fiorucci, S. Mari, and A. Fioravanti, "A new convolutional neural network-based system for NILM applications," *IEEE Trans. Instrum. Meas.*, vol. 70, 2021, Art. no. 1501112.

[2] J. Alcala, J. Urena, A. Hernandez, and D. Gualda, "Event-based energy disaggregation algorithm for activity monitoring from a single-point sensor," *IEEE Trans. Instrum. Meas.*, vol. 66, no. 10, pp. 2615–2626, Oct. 2017.

[3] Y.-H. Lin and M.-S. Tsai, "Development of an improved time–frequency analysis-based nonintrusive load monitor for load demand identification," *IEEE Trans. Instrum. Meas.*, vol. 63, no. 6, pp. 1470–1483, Jun. 2014.

[4] S. R. Shaw, S. B. Leeb, L. K. Norford, and R. W. Cox, "Nonintrusive load monitoring and diagnostics in power systems," *IEEE Trans. Instrum. Meas.*, vol. 57, no. 7, pp. 1445–1454, Jul. 2008.

[5] S. B. Leeb, S. R. Shaw, and J. L. Kirtley, "Transient event detection in spectral envelope estimates for nonintrusive load monitoring," *IEEE Trans. Power Del.*, vol. 10, no. 3, pp. 1200–1210, Jul. 1995.

[6] D. H. Green, S. R. Shaw, P. Lindahl, T. J. Kane, J. S. Donnal, and S. B. Leeb, "A MultiScale framework for nonintrusive load identification," *IEEE Trans. Ind. Informat.*, vol. 16, no. 2, pp. 992–1002, Feb. 2020.

[7] D. B. B. de Deus, C. A. N. Sobrinho, F. A. Belo, A. V. Brito, J. G. G. de Souza Ramos, and A. C. Lima-Filho, "Density of maxima approach for broken bar fault diagnosis in low slip and variable load conditions of induction motors," *IEEE Trans. Instrum. Meas.*, vol. 69, no. 12, pp. 9797–9804, Dec. 2020.

[8] M. A. Ahajjam, D. B. Licea, C. Essayeh, M. Ghogho, and A. Kobbane, "MORED: A Moroccan buildings' electricity consumption dataset," *Energies*, vol. 13, no. 24, p. 6737, 2020. [Online]. Available: https://www.mdpi.com/1996-1073/13/24/6737

[9] R. Medico *et al.*, "A voltage and current measurement dataset for plug load appliance identification in households," *Sci. Data*, vol. 7, no. 1, pp. 1–10, Feb. 2020, doi: 10.1038/s41597-020-0389-7.

[10] M. Kahl, A. Haq, T. Kriechbaumer, and H. Jacobsen, "Whited—A worldwide household and industry transient energy data set," in *Proc. 3rd Int. Workshop Non-Intrusive Load Monit.*, 2016, pp. 1–4.

[11] L. Pereira, M. Ribeiro, and N. Nunes, "Engineering and deploying a hardware and software platform to collect and label non-intrusive load monitoring datasets," in *Proc. Sustain. Internet ICT Sustainability (SustainIT)*, 2017, pp. 1–9.

[12] B. Griffith. *How to Measure Inrush AC Current*. Accessed: Jul. 1, 2019. [Online]. Available: https://community.keysight.com/community/keysight-blogs/general-electronics-measurement/blog/2018/05/23/how-to-measure-inrush-ac-current

[13] Pacific Power. *Peak Current Surge/Inrush Measurement & Programmable Phase Angle Execution for the UPC-1/3 Programmable Controller*. Accessed: Jul. 1, 2019. [Online]. Available: http://pacificpower.com/Resources/Documents/DS4PEACKCURRENT092012.pdf

[14] M. N. Meziane, T. Picon, P. Ravier, G. Lamarque, J. Le Bunetel, and Y. Raingeaud, "A measurement system for creating datasets of on/off-controlled electrical loads," in *Proc. IEEE 16th Int. Conf. Environ. Electr. Eng. (EEEIC)*, Jun. 2016, pp. 1–5.

[15] D. P. B. Renaux *et al.*, "A dataset for non-intrusive load monitoring: Design and implementation," *Energies*, vol. 13, no. 20, p. 5371, Oct. 2020. [Online]. Available: https://www.mdpi.com/1996-1073/13/20/5371

[16] D. Renaux *et al.*, "Designing a novel dataset for non-intrusive load monitoring," in *Proc. 8th Brazilian Symp. Comput. Syst. Eng. (SBESC)*, Nov. 2018, pp. 243–249.

[17] X. A. Morera and A. G. Espinosa, "Modeling of contact bounce of AC contactor," in *Proc. 5th Int. Conf. Electr. Mach. Syst. (ICEMS)*, vol. 1, Aug. 2001, pp. 174–177.

[18] E. K. Saathoff, S. R. Shaw, and S. B. Leeb, "Line impedance estimation," *IEEE Trans. Instrum. Meas.*, vol. 70, pp. 1–10, 2021.

[19] J. Paris, J. S. Donnal, Z. Remscrim, S. B. Leeb, and S. R. Shaw, "The sinefit spectral envelope preprocessor," *IEEE Sensors J.*, vol. 14, no. 12, pp. 4385–4394, Dec. 2014.

[20] E. K. Saathoff, Z. J. Pitcher, S. R. Shaw, and S. B. Leeb, "Inrush current testing," in *Proc. IEEE Appl. Power Electron. Conf. Exposit. (APEC)*, Mar. 2020, pp. 2319–2326.

[21] C. Laughman, "Fault detection methods for vapor-compression air conditioners using electrical measurements," Ph.D. dissertation, Massachusetts Inst. Technol., Cambridge, MA, USA, 2008.

[22] Terrabloom. *ECMF-250 SpecSheet*. Accessed: Apr. 10, 2021. [Online]. Available: https://cdn.shopify.com/s/files/1/0939/2046/files/ECMF-250_-_SpecSheet.% pdf

[23] P. Yin and M. B. Pate, "Impact of duct flow resistance on residential heating and cooling energy use in systems with PSC and ECM blowers," *Energy Buildings*, vol. 130, pp. 625–636, Oct. 2016.

[24] B. Stephens, A. Novoselac, and J. Siegel, "The effects of filtration on pressure drop and energy consumption in residential HVAC systems (RP-1299)," *HVAC&R Res.*, vol. 16, no. 3, pp. 273–294, May 2010.

Erik K. Saathoff (Graduate Student Member, IEEE) received the B.S. degree in electrical engineering with a minor in physics from the University of Illinois at Urbana-Champaign, Urbana, IL, USA, in 2018, and the M.S. degree in electrical engineering and computer science from the Massachusetts Institute of Technology, Cambridge, MA, USA, in 2021, where he is currently pursuing the Ph.D. degree in electrical engineering and computer science.

His research interests include high-performance power electronics, switched-capacitor converters, and system identification.

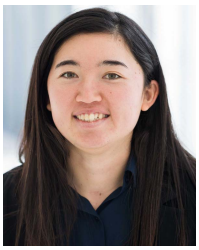

Daisy H. Green (Graduate Student Member, IEEE) received the B.S. degree from the University of Hawai'i at Mānoa, Honolulu, HI, USA, in 2015, and the M.S. degree in electrical engineering from the Massachusetts Institute of Technology, Cambridge, MA, USA, in 2018, where she is currently pursuing the Ph.D. degree.

Rebecca A. Agustin received the B.S. and M.Eng. degrees in electrical engineering and computer science from the Massachusetts Institute of Technology, Cambridge, MA, USA, in 2019 and 2021, respectively.

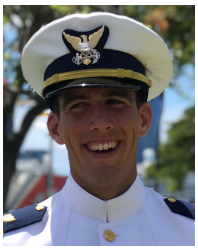

Joseph W. O'Connell received the M.S. degree in mechanical engineering from the Massachusetts Institute of Technology, Cambridge, MA, USA, in 2021.

He was previously stationed as the Auxiliary division officer aboard United States Coast Guard Cutter (USCGC) HEALY and as the Assistant Engineer Officer onboard USCGC KIMBALL. He is currently a Lieutenant with the U.S. Coast Guard, stationed as a Port Engineer.

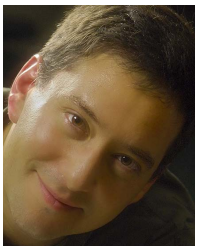

Steven B. Leeb (Fellow, IEEE) received the Ph.D. degree from the Massachusetts Institute of Technology, Cambridge, MA, USA, in 1993.

He has served as a Commissioned Officer in the United States Air Force (USAF) reserves, and he has been a member of the M.I.T. Faculty with the Department of Electrical Engineering and Computer Science since 1993. He also holds a joint appointment with the MIT's Department of Mechanical Engineering. He is the author or coauthor of over 200 publications and 20 US Patents in the fields of electromechanics and power electronics.